Biochimica et Biophysica Acta 1797 (2010) 314–323

Contents lists available at ScienceDirect

Biochimica et Biophysica Acta

journal homepage: www.elsevier.com/locate/bbabio

Mitochondrial Complex I decrease is responsible for bioenergetic dysfunction in K-ras transformed cells

Alessandra Baracca [a], Ferdinando Chiaradonna [b], Gianluca Sgarbi [a], Giancarlo Solaini [a], Lilia Alberghina [b,*], Giorgio Lenaz [a,*]

[a] Department of Biochemistry "G. Moruzzi", University of Bologna, Bologna, Italy
[b] Department of Biotechnology and Biosciences, University of Milano-Bicocca, Milan, Italy

ARTICLE INFO

Article history:
Received 14 October 2009
Received in revised form 6 November 2009
Accepted 12 November 2009
Available online 18 November 2009

Keywords:
K-ras
Cancer
Mitochondria
Respiration
ATP synthesis
Complex I

ABSTRACT

Many cancer cells are characterized by high rate of glycolysis and reduced rate of aerobic respiration, whose mechanism is still elusive. Here we investigate the down-regulation of oxidative phosphorylation (OXPHOS) in K-ras transformed mouse fibroblasts as compared to a control counterpart. Transcriptional analysis showed different expression levels of several OXPHOS nuclear genes in the two cell lines. In particular, during the exponential growth phase most genes encoding proteins of Complex I were expressed at lower levels in transformed cells. Consistently, a significant decrease of Complex I content was found in transformed cells. Moreover, analysis of NAD-dependent respiration and ATP synthesis indicated a strong decrease of Complex I activity in the mitochondria from neoplastic cells, that was confirmed by direct assay of the enzyme redox activity. At variance, succinate-dependent respiration and ATP synthesis were not significantly affected. Taken together, our results provide the new insight that the reduction of respiration observed in K-ras transformed cells is specifically due to a Complex I activity decrease.

1. Introduction

Many tumours [1,2] are characterized by a high rate of glycolysis with production of lactate even in the presence of oxygen, and by a reduced rate of aerobic respiration, the so-called Warburg effect [3]. This metabolic switch may be of advantage for tumor cells because the rate of ATP production is higher even if its efficiency is considerably lower [4]; in addition blockade of the complete oxidation of pyruvate saves precursors for biosynthetic pathways that are required for rapid growth of the tumour [5] and induces accumulation of metabolites that activate genes important for tumour progression [6]. The enhanced glycolysis accompanied by decreased OXPHOS is not the case for all tumours [1,7] and several excised tumours use more OXPHOS than glycolysis [2].

Several explanations have been proposed as molecular basis of the Warburg effect. Cancers may be prevailingly glycolytic because they are hypoxic [2]. Hypoxia due to rapid tumour growth stimulates the expression of the transcriptional factor HIF-1α (hypoxia-inducible factor-1α subunit) that induces transcription of glycolytic enzymes [8]; the concomitant decrease of mitochondrial respiration has been thought to be a direct consequence of the HIF-1α increase, since the enhanced expression of pyruvate dehydrogenase kinase inhibits pyruvate dehydrogenase and decreases carbon input into the Krebs cycle [9]. At the same time, however, HIF-1 causes a switch in the nuclear-encoded subunit 4 of cytochrome oxidase from the isoform COX4-1 to COX4-2 resulting in more efficient electron delivery to oxygen [10,11]. Nevertheless, a decrease of the respiratory chain activity has been observed in several tumours [12]. This latter observation has brought to postulate an opposite sequence of events, with reduction of respiration preceding a compensatory increase of glycolysis. In favour of the second interpretation there is the observation of a mitochondrial dysfunction due to transcriptional deregulation of several mitochondrial proteins [13,14]. In this scenario, p53 mutations, frequently observed in cancer, have been proposed to represent the primary cause of respiration decrease by preventing the correct assembly of cytochrome oxidase [15]. Recent studies indicate that mitochondrial dysfunction is one of the more recurrent features of cancer cells [16,12], as reported at microscopic, molecular, biochemical, and genetic level [17-19]. Mitochondrial

Abbreviations: OXPHOS, oxidative phosphorylation; HIF-1, hypoxia-inducible factor-1; DNP, dinitrophenol; RH-123, Rhodamine-123; TMRM, tetramethylrhodamine methylester; MitoTracker Red, chloromethyl-X-rosamine (CMX-Ros); $\Delta\Psi_m$, mitochondrial electrical membrane potential; ROS, reactive oxygen species

* Corresponding authors. G. Lenaz is to be contacted at Department of Biochemistry "G. Moruzzi", University of Bologna, Via Irnerio 48, 40126 Bologna, Italy. Tel.: +39 051 2091229; fax: +39 051 2091217. L. Alberghina, Department of Biotechnology and Biosciences, University of Milano-Bicocca, Piazza della Scienza 2, 20126 Milan, Italy. Tel.: +39 02 64483515; fax: +39 02 64483519.
E-mail addresses: lilia.alberghina@unimib.it (L. Alberghina), giorgio.lenaz@unibo.it (G. Lenaz).

0005-2728/$ – see front matter © 2009 Elsevier B.V. All rights reserved.
doi:10.1016/j.bbabio.2009.11.006

DNA mutations, extremely frequent in cancer cells, have also been involved in the generation of mitochondrial abnormalities [18,20].

Although cancer cells under several conditions, including hypoxia, oncogene activation, mDNA mutation [21-23], may substantially differ in their ability to use oxygen, only few reports have been able to identify a strict association between metabolic changes in cancer cells and mitochondrial complexes composition and activity. For example, in renal oncocytomas [24] the NADH dehydrogenase activity and protein content of Complex I were found to be strongly depressed; subsequently, in a thyroid oncocytoma cell line [25] a similar decrease of Complex I activity was ascribed to a specific mutation in the ND1 gene of mitochondrial DNA. In some hereditary tumours (renal cell carcinomas) a correlation has been identified between mitochondrial dysfunctions and content of OXPHOS complexes [26]. For example, the low content of Complex V, often observed in clear cell type renal cell carcinomas and in chromophilic tumours, seems to indicate that the mitochondria were in an inefficient structural and functional state [26]. However, it cannot be excluded that, in some cases, the structural alteration of Complex V may offer a functional advantage to cells exhibiting a deficient respiratory chain [27]. Moreover, recent experimental evidence has shed some light on a pivotal role of mitochondrial morphology in the control of important mitochondrial functions such as apoptosis [28] and oxidative phosphorylation [29]. In particular, dysregulated mitochondrial fusion and fission events can now be regarded as playing an important role in cancer onset and maintaining [30]. At present, however, a reliable understanding is still lacking of the role, if any, that mitochondria play in neoplastic transformation.

In order to critically analyze the molecular basis of the change of carbon metabolism in cancer cells, in this study we compare two cell lines that have been previously characterized [13,14, 31,32], that is NIH3T3 mouse fibroblasts (that we refer to as control, or C) and NIH3T3 cells transformed by an activated form of the K-ras oncogene [32,33] (that we refer to as transformed, or T). Ras proteins are intracellular switches whose activation state (i.e. their binding to GDP or GTP) controls downstream pathways leading to cell growth and differentiation. The activation state of Ras proteins is governed through the competing action of GTPase Activating Proteins (GAP) and Guanine nucleotide Exchange Factors (GEF). Mutation of the ras gene is a critical event in the onset of different malignant phenotypes [34]. Also deregulation of either GAP or GEF activity may result in hypo-or hyper-activation of downstream pathway(s), so that for instance over-expression of a GEF or inactivation of a GAP may both result in cell transformation [35,36].

Cells harbouring k-ras mutations were consistently found to have an increased expression of the glucose transporter GLUT1 and an enhanced glycolytic rate, presumably as a compensation to glucose deprivation [37]. In this study we show that the major phenotypic change of T fibroblasts is a dramatic loss of activity and content of respiratory Complex I (NADH-CoQ oxidoreductase), resulting in a strong decrease of both NAD-linked respiration and ATP synthesis rate. Accordingly, a significant change in the expression of several genes encoding subunits of the mitochondrial oxidative phosphorylation complexes, and in particular of Complex I, was observed in T cells.

2. Materials and methods

2.1. Cell culture

Control mouse fibroblasts (obtained from the ATCC, Manassas, VA, USA) and K-Ras-transformed normal derived cell line, 226.4.1 [38] were routinely grown in Dulbecco's modified Eagle's medium containing 10% Fetal Bovine Serum (FBS), 4 mM glutamine, 100 U/ml penicillin, 100 mg/ml streptomycin and 0.25 mg/ml amphotericin B at 37 °C in a humidified atmosphere of 5% CO_2. Growth curves and ATP levels of cells were obtained by seeding 6×10^4 cells in DMEM containing either glucose 25 mM or 1 mM, 110 mg/l pyruvate, 4 mM glutamine, and supplemented with 10% FBS. To enhance potential alterations in respiratory chain-dependent ATP synthesis cells were grown in DMEM glucose-free medium containing 5 mM galactose, 110 mg/l pyruvate, and 4 mM glutamine, supplemented with 10% dialyzed fetal bovine serum. The growth ability of cell lines was assayed by changing daily the culture medium and counting cells till 72 h.

2.2. RNA preparation and Affymetrix Analysis

To probe the global gene expression in our fibroblasts, along a time course, RNA was extracted as described previously [14] and mouse genome 430 2.0 array Affymetrix (Affymetrix, Santa Clara, CA) were used. The mouse genome 430 2.0 array is a high-density oligonucleotide array comprised of over 45,101 probe sets representing over 34,000 well-substantiated mouse genes. For all the experiments we used MAS5 pre-processing method with default parameters. Expression analysis files originated from each sample (chip) were then imported in GeneSpring 7.3.1 (Silicon Genetics) for further analysis. In particular, for the normalization procedure, probe-set values below 0.01 were placed to 0.01. Normalization was performed by using a per-chip 50th percentile method that normalizes each chip on its median, allowing comparison among chips and using per-gene normalization where the measurement of each probe was normalized to the median of the measurements of that probe in the different chips. For the analysis of the data, a cross-gene error model was applied. Further standard filtering procedures were applied (i.e. Flag had to be indicated as “Present” in at least one sample of the time course; the samples with an intensity value below 50 units were excluded; the genes showing a standard deviation between 0 and 1 in at least 85% of the samples were selected). Moreover, transcriptional data obtained for the genes of each mitochondrial Complex, have been analyzed through unsupervised hierarchical clustering (as implemented in the GeneSpring platform). The results of this process are the dendrograms (one for each Complex), that typically unsupervised hierarchical clustering procedure provides.

2.3. Mitochondrial ATP synthesis assay and cellular ATP content

The oligomycin-sensitive ATP synthase activity in permeabilized cells was determined according to the method described by Sgarbi et al. [39]. Essentially, fibroblasts (3×10^6 cells/ml) were incubated for 12 min with 60 μg/ml digitonin in a Tris/Cl buffer (pH 7.4). Complex I and Complex II driven ATP synthesis was induced by adding 10 mM glutamate /10 mM malate (+0.6 mM malonate) or 20 mM succinate (+4 μM rotenone) and 0.5 mM ADP (all reagents were from Sigma-Aldrich, St. Louis, MO, USA) to the sample. After 5 min the reaction was stopped by adding dimethylsulphoxide (80%) to the sample and the ATP content was measured by the luciferine/luciferase chemiluminescent method.

2.4. Respiration measurements

Oxygen consumption rates were measured in permeabilized cells (60 μg/ml digitonin) at 30 °C using an oxygen Clark-type electrode as previously reported by Baracca et al. [40]. State 4 respiration rates were determined by adding to cell samples 20 mM succinate (plus 4 μM rotenone) or 10 mM glutamate/10 mM malate (plus 1.8 mM malonate). State 3 and uncoupled respiration rates were measured in the presence of 0.8 mM ADP or 60 μM DNP (dinitrophenol),

respectively. NADH-dependent and succinate-dependent respirations were sensitive to rotenone and malonate, respectively.

2.5. Mitochondria isolation

We set a simple method allowing to obtain a high mitochondria yield. Cells were harvested, washed once in PBS (1 mM KH_2PO_4, 3 mM Na_2HPO_4, 154 mM NaCl), and resuspended (10 mg/ml) in 10 mM Tris/Cl buffer (pH 7.4) containing 1 mM PMSF (phenylmethanesulfonyl fluoride) and 0.5 mg/ml digitonin. After 7 min in ice an equal volume of buffer (140 mM sucrose, 440 mM mannitol, 40 mM HEPES, 2 mM EDTA, 200 μM EGTA and 1 mM PMSF) was added to the cells and the suspension was centrifuged at 600g for 10 min in a refrigerated centrifuge (Beckman Avanti J-25 centrifuge equipped with a JA18.1 rotor). The supernatant was decanted and the pellet was resuspended (10 mg/ml) in 10 mM Tris/Cl buffer (pH 7.4) containing 1 mM PMSF and 2.5 mg/ml digitonin and kept in ice for 10 min. The permeabilized cell suspension was again diluted and centrifuged as above. The supernatant mitochondrial fraction was then centrifuged at 10,000g for 10 min in the refrigerated Beckman centrifuge. Finally, mitochondria were washed once in buffer (70 mM sucrose, 220 mM mannitol, 20 mM HEPES, 1 mM EDTA, 100 μM EGTA and 1 mM PMSF) and resuspended at 3–4 mg protein/ml in 20 mM HEPES/KOH buffer containing 250 mM sucrose, 1 mM EDTA and 100 μM EGTA, pH 7.4. The mitochondrial protein yield was about 4%.

2.6. Complex I redox activity

NADH-CoQ oxidoreductase activity was measured in daily isolated fresh mitochondria suspension (3.5 mg/ml) exposed to 3 cycle of sonic radiation. The enzyme activity (30 °C) was assayed at substrates' saturating concentration (75 μM NADH; 80 μM decylubiquinone) and in the presence of 1.8 μM Antimycin A and 2 mM KCN to inhibit Complex III and Complex IV, respectively. The rotenone sensitive NADH-CoQ oxidoreductase activity (i.e. the mitochondrial redox activity was 95% inhibited in the presence of 2 μM rotenone) was detected following the decrease of NADH absorption at 340 – 380 nm in a JASCO V550 UV-VIS dual wavelength spectrophotometer equipped with a mixing apparatus. The molar absorbance coefficient used for NADH was 4.1 mM^{-1} cm^{-1}.

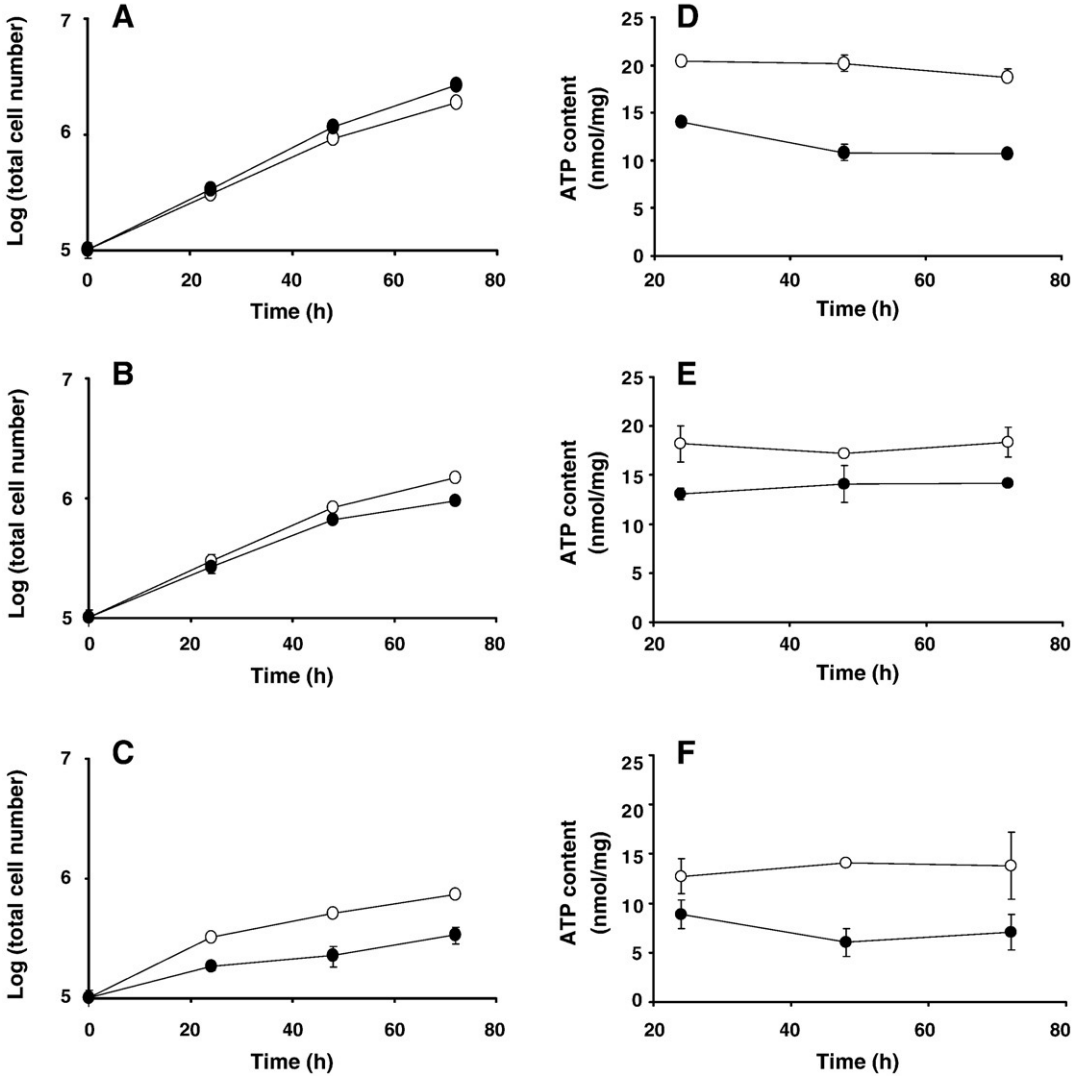

Fig. 1. Cell growth and ATP level of control and transformed cells. Cell growth (A, B, C) and ATP level (D, E, F) of control (open circles) and transformed cells (filled circles) cultured for 72 h changing the medium daily. Cells were incubated in DMEM containing 25 mM glucose (A, D), 1 mM glucose (B, E) or 5 mM galactose to substitute for glucose (C, F), 110 mg/l pyruvate, 4 mM glutamine, and supplemented with either 10% FBS or dialyzed FBS when cells were cultured in galactose medium. The data are averages ± SD from one of two independent experiments, each performed in triplicate (when not seen, SD was within the circle diameter).

2.7. Citrate synthase assay

Citrate synthase activity and cell sample protein concentration were determined as previously described [41].

2.8. Mitochondrial membrane potential analysis in living cells

Fluorescence micrographs of oligomycin-treated (state 4 respiratory condition) and untreated (state 3) adherent permeabilized-cells were obtained using the tetramethylrhodamine methylester (TMRM) (Molecular Probes) fluorescent probe as reported in Solaini et al. [42]. Images were acquired using a fluorescence inverted microscope (Olympus IX50 equipped with a CCD camera). Multiple high-power (20×) images were acquired with IAS2000 software (Delta Sistemi, Italy). To quantitate $\Delta\Psi_m$ under different metabolic conditions, steady-state fluorescence quenching measurements of permeabilized cells incubated with rhodamine 123 (RH-123) (Molecular Probes) were carried out as described [41,42].

Mitochondrial potential in intact cells was determined with the probe CMX-Ros (MitoTracker Red) (Molecular Probes) using fluorescence-activated cell sorter (FACScan, Becton-Dickinson). Briefly, cells were trypsinized by treatment with 0.25% trypsin, then were suspended in 1 ml of PBS + 10% FCS (0.5×10^6 cells per analysis) containing the dye (60 nM) and labeled for 30 min at 37 °C in the dark. The unbound dye was then removed with one wash and promptly used for flow cytometric analysis. The percentage and the mean value of potential was calculated for each sample and corrected for autofluorescence obtained from samples of unlabeled cells. Data analysis was performed with WinMDI software.

2.9. OXPHOS complexes immunodetection and supercomplex organization

To evaluate the OXPHOS complexes content, cellular homogenates were electrophoretically separated by SDS-PAGE and blotted on nitrocellulose membrane. The OXPHOS complexes estimation was based on immunodetection and quantification of single subunit of each protein complex. Supercomplex organization of respiratory complexes was analyzed in isolated digitonin-treated mitochondria by 1D blue-native PAGE followed by 2D SDS-PAGE [19]. The protein electrophoretic pattern obtained under denaturating conditions were then electroblotted onto nitrocellulose membrane. The four protein complexes were detected and quantified by a chemiluminescent technique based on the ECL™Western Blotting Detection Reagent Kit

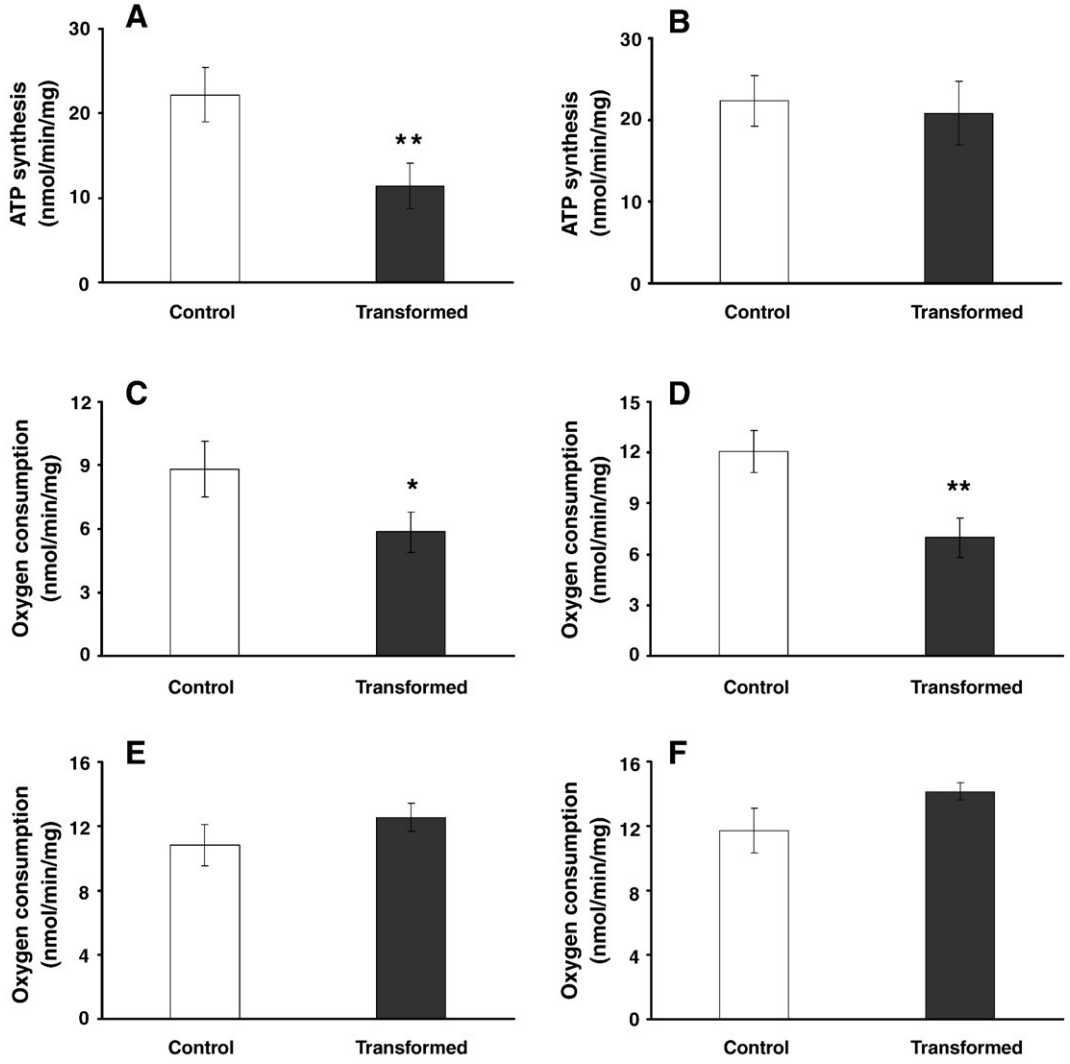

Fig. 2. Mitochondrial ATP synthesis and oxygen consumption rates measured in digitonin-permeabilized cells grown for 48 h in glucose enriched medium. ATP synthesis rates were determined in presence of glutamate-malate (A) and succinate (B) as respiratory substrates. Oxygen consumption rates were measured in cells energized with both Complex I -(C, D) and Complex II- (E, F) dependent substrates under state 3 (C, E) and uncoupled (D, F) respiratory conditions. The data are averages+/-SD of three independent experiments. Data were considered significantly different when $P \leq 0.05$ (*) or $P \leq 0.01$ (**).

(Amersham Biosciences, Piscataway, NJ, USA) using a cocktail of primary monoclonal antibodies specific for single subunits of each respiratory complex as follows: NDUFA9 (39 kDa) of Complex I, SDHA (70 kDa) of Complex II, Rieske protein (22 kDa, apparent molecular weight is 30 kDa) of Complex III, COX-I (57 kDa, apparent 45 kDa) of Complex IV (MitoSciences Inc., Eugene, OR, USA) and a secondary goat anti-mouse IgG_{H+L} antibody labeled with horseradish peroxidase (Molecular Probes, Eugene, OR, USA). The molecular mass scale of the 1D electrophoresis was drawn on the basis of standard proteins (HMW calibration kit for Native electrophoresis, Amersham Biosciences).

2.10. Statistical analysis

All statistical analyses were performed with OriginPro 7.5 (OriginLab Corporation, MA, USA), using unpaired Student's *t* test between groups. Data show mean ± SD. Groups were considered significantly different when $P \leq 0.05$ (*) or $P \leq 0.01$ (**).

3. Results

3.1. Cell growth and mitochondrial function

In order to highlight a possible bioenergetics impairment of transformed fibroblasts as compared to control ones, cell proliferation was studied under different conditions of glucose availability (25 mM, 1 mM) and in absence of glucose (substituted by 5 mM galactose). In particular, the proliferation ability of the two cell lines was assayed by changing daily the culture medium and counting cells till 72 h. As shown in Fig. 1A, in 25 mM glucose, both lines grew linearly on a semilog plot for nearly 48 h (from now on called "exponential growth phase"), but ras-transformed cells had a

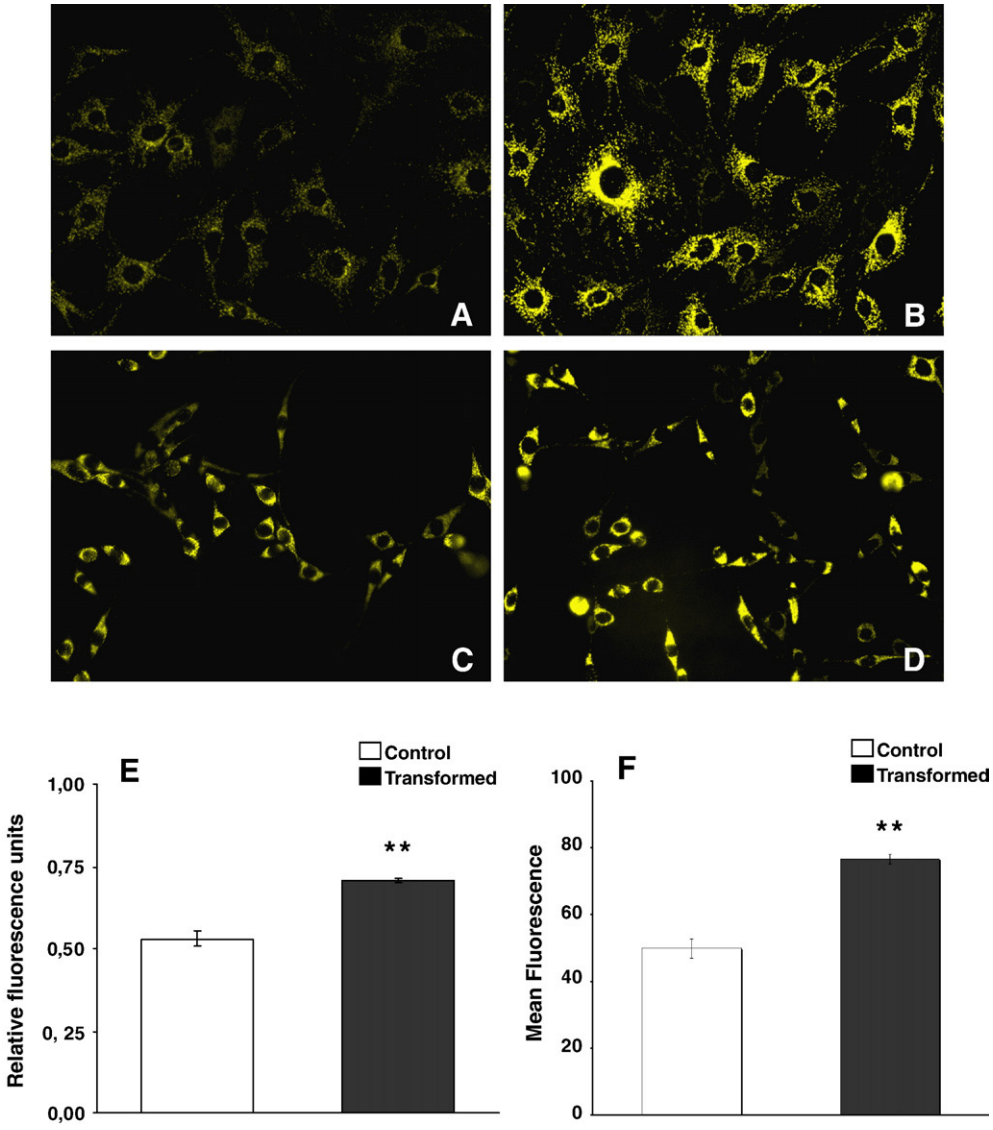

Fig. 3. Mitochondrial membrane potential of K-ras transformed fibroblasts. Typical fluorescence microscopy images of TMRM-loaded digitonin permeabilized cells under different metabolic conditions (A, C state 3 and B, D state 4 respiration) obtained from control (A, B) and transformed (C, D) cells grown for 48 h in 25 mM glucose medium. (E) Fluorescence quenching initial rate measurements of rhodamine 123 (RH-123) in digitonin-permeabilized cells under state 3 respiratory conditions. Histogram shows the mean values ± SD of three independent experiments. Data were considered significantly different when $P \leq 0.05$ (*) or $P \leq 0.01$ (**). (F) Analysis of mitochondrial potential in control and transformed cells. Cells, cultured in 25 mM glucose enriched medium for 48 h, were *in vivo* stained with MitoTracker Red and then analyzed by FACS. Data are reported as mean fluorescence of stained population-Mean Fluorescence-. Histogram shows the mean values ± SD of three independent experiments. Data were considered significantly different when $P \leq 0.05$ (*) or $P \leq 0.01$ (**).

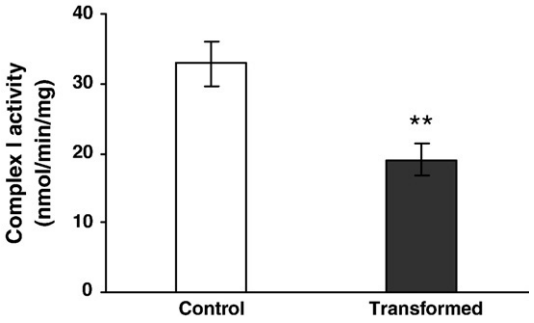

Fig. 4. Mitochondrial Complex I redox activity in control and transformed cells. The NADH-Ubiquinone oxidoreductase activity was measured in fresh mitochondria isolated daily from both cell lines. The cells were cultured in 25 mM glucose medium for 48 h before isolating mitochondria. The data are averages ± SD of three independent experiments. Data were considered significantly different when $P \leq 0.05$ (*) or $P \leq 0.01$ (**).

growth yield higher as compared to control cells. By decreasing glucose availability (and consequently glycolysis rate) ras-transformed cells grew much more slowly than control cells (Fig. 1B and C), resulting at 72 h in a yield ratio (cell yield in 25 mM glucose/cell yield in 5 mM galactose) of about 8, whereas the same ratio scored nearly 3 when estimated for wild-type cells. Similar results (not shown) were also obtained mimicking the *in vivo* limited nutrients availability of tumour cells by changing the culture medium only once (at zero time). This behavior suggested an impairment of OXPHOS in transformed cells. Incidentally, the ATP level (nmol/mg cell protein) was found to be lower in ras-transformed than in control fibroblasts, and this event occurred independently of culture conditions (Fig. 1D–F). Since ATP level is set by the steady state balance of ATP synthesis and ATP utilization rates that may both vary in transformed cells, only measurements of ATP synthesis rates could detect mitochondrial impairment. Therefore we investigated functional and structural features of the oxidative phosphorylation system. Moreover, in order to define possible mitochondrial dysfunctions in K-ras transformed cells, and with the hope to elucidate the K-ras activated/repressed pathways, the OXPHOS transcriptional profiling has been analyzed.

3.2. Respiratory activity and oxidative phosphorylation in digitonin-permeabilized cells

Citrate synthase activity expressed as nmol/min/mg protein was determined and found not significantly changed in ras-transformed cells as compared to control cells (C cells: 202.17 ± 16.32; T cells: 189.85 ± 17.96); being independent on the glucose concentration of the culture medium (data not shown). Such findings indicate that the average mitochondrial mass per cell is not modified by transformation. The ATP synthesis rate of permeabilized transformed cells was strongly decreased (almost 50%) with respect to controls when glutamate-malate but not succinate was the respiratory substrate (Fig. 2A and B). This finding indicates that a specific deficit is present at the level of Complex I of the respiratory chain, whereas the other respiratory complexes and the ATP synthase are not significantly affected. Likewise, the measurement of oxygen consumption of cells grown 48 h in high glucose in State 4 (controlled state, without ADP addition) did not show significant changes (data not shown), while a decrease of both State 3 (under phosphorylating conditions) and dinitrophenol-induced uncoupled respiration was observed with glutamate-malate as substrates in transformed cells (Fig. 2C and D). A decrease of respiratory control ratio was exclusively a consequence of decreased State-3 respiration. In agreement with data of ATP synthesis rate, under State 3 and uncoupled respiratory conditions the succinate-sustained oxygen consumption by transformed and control cells was very close (Fig. 2E and F).

By means of fluorescence microscopy, we have also measured the mitochondrial transmembrane potential using the TMRM probe in permeabilized cells. In agreement with previously reported findings [14], ras-transformed fibroblasts presented different morphology with respect to wild-type fibroblasts (Fig. 3 compare upper panels with lower panels). Mitochondria energized with glutamate–malate exhibit an increased potential in ras-transformed cells as compared to control cells under State 3 conditions only (Fig. 3A and C). These data were confirmed by measuring the membrane potential with an independent approach that can provide quantitative information on the average mitochondrial membrane potential in cell populations [42]. This method is based on the evaluation of the fluorescence quenching of rhodamine 123 (RH-123). Analysis by RH-123 showed in transformed fibroblasts grown in 25 mM glucose, that under State 3 conditions the fluorescence quenching initial rate, which is directly related with mitochondrial $\Delta\Psi$ [43], is 35% higher than in control fibroblasts (Fig. 3E). MitoTracker Red staining in intact cells further confirmed this result. Indeed, transformed cells showed higher endogenous mitochondrial membrane potential than control cells (Fig. 3F). This finding is somehow unexpected in view of the lower rate of NAD-linked respiration. However, transformed cells maintained in glucose-enriched medium preferentially synthesize ATP through glycolysis than through OXPHOS, possibly determining a higher $\Delta\Psi$ as compared to control cells when it is measured in both intact cells [42] and in permeabilized cells under State 3 respiratory conditions [41,43].

3.3. Decrease of activity of Complex I in transformed cells

Given that the biochemical results shown above (Fig. 2) suggested a decrease of Complex I activity, we proceeded to its measure in mitochondria isolated from cells grown for 48 h (Fig. 4). A significant reduction of activity occurred in the transformed cells; the decrease of Complex I activity was in the range of the observed NAD-dependent respiration decrease, in line with Complex I being rate-limiting for the respiratory chain.

Since both succinate-dependent respiration and ATP synthesis in ras-transformed cells were not affected (Fig. 2), the activity of Complex II (that is rate limiting for succinate oxidation) as well as those of Complexes III, IV and V were not altered at least to an extent

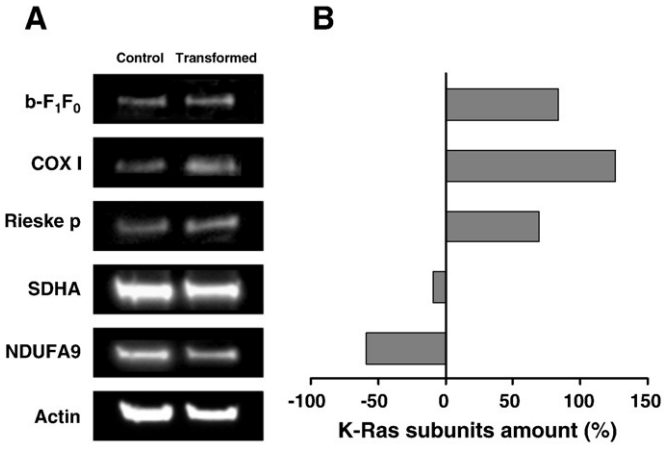

Fig. 5. Content of mitochondrial OXPHOS complexes in control and transformed cells. (A) Immunodetection of single subunits of each OXPHOS complex revealed after SDS-PAGE separation. (B) Histogram (right) shows the densitometric analysis of OXPHOS subunits in transformed compared to control cells. Analysis of each band was obtained with the Quantity One software (BioRad) using Actin as internal standard.

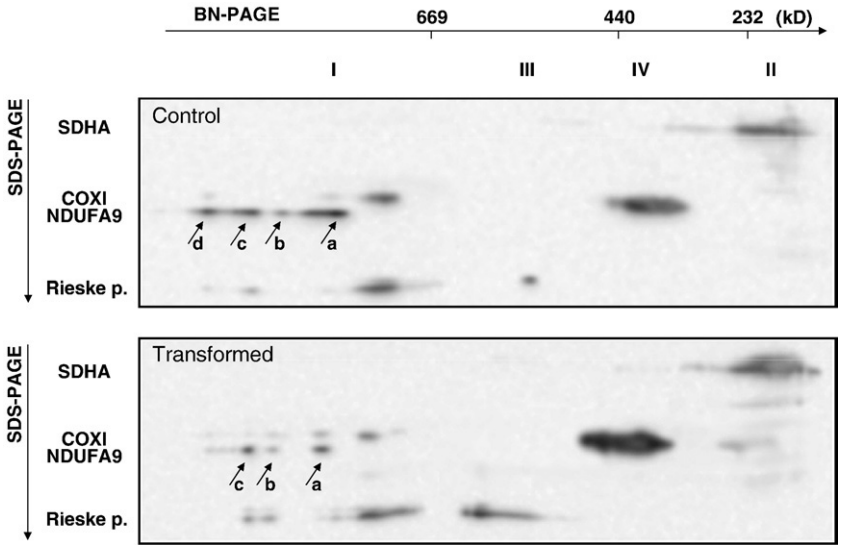

Fig. 6. Two-dimensional separation of mitochondrial respiratory supercomplexes from control (Top) and transformed (Bottom) cells. Supercomplexes separation was achieved by 1D Blue-Native electrophoresis followed by 2D SDS-PAGE. 2D gels were blotted onto nitrocellulose membrane and then exposed to a cocktail of monoclonal antibodies specific for single subunits of each respiratory complex. Protein bands of molecular mass above 1000 kDa (a, monomeric Complex I) are: b, I + III + IV: supercomplex formed by complex I, III and IV (K-ras cells only); c, I + III: supercomplex formed by complex I and III; d, I + III + IV supercomplex formed by complex I, III, and IV (normal cells only). Incidentally, in the control cell gel, band b results from an aggregate of proteins that includes complex I, but none of the other respiratory chain complexes.

sufficient to become the rate-limiting step. The content of mitochondrial complexes was investigated in cell homogenates by gel electrophoresis under denaturing conditions followed by western blotting and immunodetection of OXPHOS complexes subunits (Fig. 5A and B). A significant increase of the content of Complex III, Complex IV and ATP synthase was observed in transformed cells with respect to wild type, while Complex II was unchanged. At variance, transformed cells showed a reduction of approximately 50% of Complex I content (Fig. 5B). Moreover, 2-D electrophoretic analysis of supercomplexes organization, while confirming the depletion of Complex I in transformed cells, showed the disappearance of the highest molecular weight supercomplex composed by complexes I, III and IV (Fig. 6).

3.4. Transcriptional profiling of nuclear genes involved in oxidative phosphorylation

In order to extend at a molecular genome-wide level the characterization of control and K-ras transformed fibroblasts, the time-dependent transcriptional profiling of the two sets of mouse fibroblasts was performed. The transcriptional analysis was performed between 0 h and 72 h, because in this time interval both cell lines did not run out glucose from the medium ([13] and unpublished observations). Incidentally, transcriptional analysis of glycolytic genes was previously performed [13] showing enhanced transcription of genes for several glycolytic enzymes in T cells grown in high glucose medium.

3.4.1. Complex I

We identified and analysed the expression of 31 nuclear genes (out of 39) encoding subunits of Complex I (Fig. 7A). Interestingly, in control cells the level of expression of most genes encoding subunits of Complex I increased along the time course, whereas in transformed cells the expression of 12 genes only were found enhanced with time, and many genes were less expressed. Consequently, the difference between the expression profiles was remarkable particularly at later time point (72 h) when most genes encoding subunits of Complex I were expressed at lower levels in transformed cells. This result is more clearly shown by the T/C ratio (Fig. 7B, compare 0–24 h versus 72 h), in which the green box values, representing lower expression in transformed cells, notably increased between 24 h and 72 h (16 genes were expressed at lower level). In conclusion, the reduction of the Complex I content in K-ras transformed cells was in agreement with the main differences observed in the time-dependent OXPHOS transcriptional profile of the two sets of mouse fibroblasts.

3.4.2. Complex II, III, IV and V

We identified and analyzed the expression of 43 genes encoding polypeptides of the other four OXPHOS complexes. In particular we identified 3 genes for Complex II, 9 for Complex III, 17 for Complex IV and 15 for Complex V. The transcriptional profile analysis indicated in both cell lines a time-dependent decrease of the expression level of about half the genes encoding proteins of both complexes III and IV and a general expression increase of the genes encoding proteins of complex II and V (Fig. 7A and B).

4. Discussion

The high glycolytic rate observed in several tumour cells and tissues may depend upon mitochondrial dysfunction and/or hypoxic environment of developing tumour, a condition that would force cancer cells to use essentially glycolysis to generate ATP. Mitochondrial dysfunctions are known to be caused either by mtDNA mutation and/or by aberrant expression of metabolic and mitochondrial enzymes, while hypoxia is due to low vascularization that limits

Fig. 7. OXPHOS nuclear gene expression analysis in control and transformed cells. The gene expression analysis was performed by using Affymetrix arrays. The schematic diagram represents the relative mRNA levels (Signal Log Ratio) of OXPHOS nuclear genes of control (C) and transformed (T) cells grown in 25 mM glucose containing medium. (A) Gene expression data, collected at different time points (0, 24, 48 and 72 h), were subjected to standard normalization and filtering procedures, as described in Materials and methods, allowing to identify metabolic genes that show significant statistical expression (P-value ≤ 0.05). Data are colour-coded according to the red-green colour spectrum depicted on the left of the Figure (expression) and clustered depending on the mitochondrial complex they belong. (B) T/N ratios are obtained from the gene expression profiles of the two cell lines. The values of such ratios were graphically expressed (top right) as low-green colour-when the ratio was ≤0.9, high-red colour-when the ratio was ≥1.1 and equal-yellow colour-when the ratio was between 0.9 and 1.1.

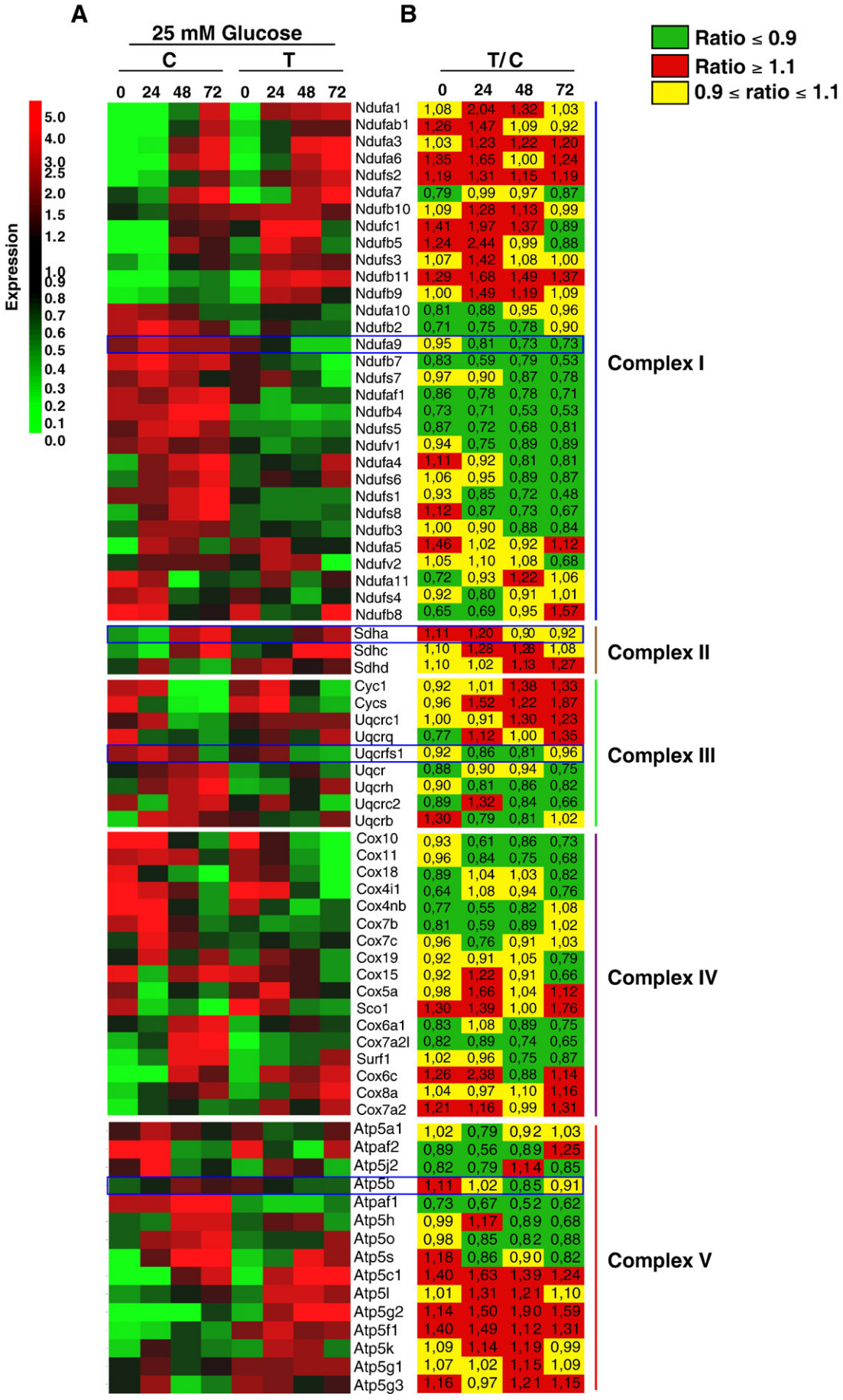
A
25 mM Glucose
C
T
0 24 48 72 0 24 48 72
Expression
5.0
4.0
3.0
2.5
2.0
1.5
1.2
1.0
0.9
0.8
0.7
0.6
0.5
0.4
0.3
0.2
0.1
0.0
B
T/C
0 24 48 72
Ratio ≤ 0.9
Ratio ≥ 1.1
0.9 ≤ ratio ≤ 1.1
Ndufa1 1,08 2,04 1,32 1,03
Ndufab1 1,26 1,47 1,09 0,92
Ndufa3 1,03 1,23 1,22 1,20
Ndufa6 1,35 1,65 1,00 1,24
Ndufs2 1,19 1,31 1,15 1,19
Ndufa7 0,79 0,99 0,97 0,87
Ndufb10 1,09 1,28 1,13 0,99
Ndufc1 1,41 1,97 1,37 0,89
Ndufb5 1,24 2,44 0,99 0,88
Ndufs3 1,07 1,42 1,08 1,00
Ndufb11 1,29 1,68 1,49 1,37
Ndufb9 1,00 1,49 1,19 1,09
Ndufa10 0,81 0,88 0,95 0,96
Ndufb2 0,71 0,75 0,78 0,90
Ndufa9 0,95 0,81 0,73 0,73
Ndufb7 0,83 0,59 0,79 0,53
Ndufs7 0,97 0,90 0,87 0,78
Ndufaf1 0,86 0,78 0,78 0,71
Ndufb4 0,73 0,71 0,53 0,53
Ndufs5 0,87 0,72 0,68 0,81
Ndufv1 0,94 0,75 0,89 0,89
Ndufa4 1,11 0,92 0,81 0,81
Ndufs6 1,06 0,95 0,89 0,87
Ndufs1 0,93 0,85 0,72 0,48
Ndufs8 1,12 0,87 0,73 0,67
Ndufb3 1,00 0,90 0,88 0,84
Ndufa5 1,46 1,02 0,92 1,12
Ndufv2 1,05 1,10 1,08 0,68
Ndufa11 0,72 0,93 1,22 1,06
Ndufs4 0,92 0,80 0,91 1,01
Ndufb8 0,65 0,69 0,95 1,57
Complex I
Sdha 1,11 1,20 0,90 0,92
Sdhc 1,10 1,28 1,28 1,08
Sdhd 1,10 1,02 1,13 1,27
Complex II
Cyc1 0,92 1,01 1,38 1,33
Cycs 0,96 1,52 1,22 1,87
Uqcrc1 1,00 0,91 1,30 1,23
Uqcrq 0,77 1,12 1,00 1,35
Uqcrfs1 0,92 0,86 0,81 0,96
Uqcr 0,88 0,90 0,94 0,75
Uqcrh 0,90 0,81 0,86 0,82
Uqcrc2 0,89 1,32 0,84 0,66
Uqcrb 1,30 0,79 0,81 1,02
Complex III
Cox10 0,93 0,61 0,86 0,73
Cox11 0,96 0,84 0,75 0,68
Cox18 0,89 1,04 1,03 0,82
Cox4i1 0,64 1,08 0,94 0,76
Cox4nb 0,77 0,55 0,82 1,08
Cox7b 0,81 0,59 0,89 1,02
Cox7c 0,96 0,76 0,91 1,03
Cox19 0,92 0,91 1,05 0,79
Cox15 0,92 1,22 0,91 0,66
Cox5a 0,98 1,66 1,04 1,12
Sco1 1,30 1,39 1,00 1,76
Cox6a1 0,83 1,08 0,89 0,75
Cox7a2l 0,82 0,89 0,74 0,65
Surf1 1,02 0,96 0,75 0,87
Cox6c 1,26 2,38 0,88 1,14
Cox8a 1,04 0,97 1,10 1,16
Cox7a2 1,21 1,16 0,99 1,31
Complex IV
Atp5a1 1,02 0,79 0,92 1,03
Atpaf2 0,89 0,56 0,89 1,25
Atp5j2 0,82 0,79 1,14 0,85
Atp5b 1,11 1,02 0,85 0,91
Atpaf1 0,73 0,67 0,52 0,62
Atp5h 0,99 1,17 0,89 0,68
Atp5o 0,98 0,85 0,82 0,88
Atp5s 1,18 0,86 0,90 0,82
Atp5c1 1,40 1,63 1,39 1,24
Atp5l 1,01 1,31 1,21 1,10
Atp5g2 1,14 1,50 1,90 1,59
Atp5f1 1,40 1,49 1,12 1,31
Atp5k 1,09 1,14 1,19 0,99
Atp5g1 1,07 1,02 1,15 1,09
Atp5g3 1,16 0,97 1,21 1,15
Complex V

oxygen supply in growing tumours. Recently, observations point to a direct influence of activated oncogenes on the energy metabolism of tumours [15,44,45].

Here we made use of a model of immortalized mouse fibroblasts and isogenic K-ras transformed cells to investigate the correlation of oncogenic ras activation with metabolic alteration and mitochondrial (dys)function. Indeed, by using cellular models of ras transformation from different origin (human, mouse, and rat), several reports have shown the ability of oncogenic ras to alter cellular metabolism [46] as well as the presence of enhanced glycolysis [37]. However, our aim was to ascertain the possible presence of a link between the Warburg effect in our transformed cell model [13] and mitochondrial function. Therefore, we analyzed in detail several oxidative phosphorylation parameters and associate them with the expression of energy metabolism genes and level of OXPHOS complexes. Taken together our results showed a significant dysfunction of mitochondria in transformed cells that is due to a decrease of Complex I activity and consequent severe reduction of both NAD-linked respiration and ATP synthesis, which is in agreement with the notion that Complex I is rate-limiting over the respiratory chain [19].

The Complex I impairment well correlates with the transcriptional profiles of transformed cells. Indeed at 48 h, time at which the mitochondrial functional analysis was performed, as well as at a later time point (72 h), we observed a significant reduction of the expression (T/C ratio) of most genes encoding Complex I subunits. However, the general reduction of transcription of genes encoding proteins of mitochondrial complexes (particularly complex I and IV) in transformed cells was confirmed only in part by the protein analysis. The substantial decrease of Complex I and the lack of changes of Complex II content, as detected by western blotting (Ndufa9 and Sdha, respectively), were in line with the transcriptional behaviour; whereas the significant increase of content of the other OXPHOS complexes, particularly of Complex IV, was unexpected. Indeed, in transformed cells, at 48 h, *Uqcrfs1, COX I* [14] and *Atp5b* genes were expressed at lower, equal and lower level, respectively than in controls.

Although the correlation between array and protein expression data is generally poor for mitochondrial proteins [47], a possible explanation for this discrepancy might be that ras-transformed cells have an enhanced mRNA stability. In fact OXPHOS gene expression and mRNA stability are strictly linked to respiratory activity, as demonstrated in mitochondria from patients exhibiting severe respiratory defects, that showed increased steady state levels of nuclear transcripts encoding mitochondrial OXPHOS complexes subunits [48]. Moreover mitochondrial respiratory chain complexes, once assembled are extremely stable, many having half lives of up to 9 days [49,50]; this effect may explain why the reduction of mRNA for OXPHOS genes (48 h) is not matched by the protein levels observed at the same time point.

Why then does Complex I behave in an opposite way, and the protein levels at 48 h appear to match mRNA decrease? Such effect could be ascribed to a secondary damage due to enhanced ROS production in K-ras transformed cells, as it was previously reported [13]; that is in line with the particular vulnerability of Complex I by ROS [51,52]. Moreover, it has been shown that the rate of newly synthesized mitochondrial protein degradation is significantly affected by the generation of mitochondrial free radicals [53].

An alternative explanation for the decrease of Complex I is an impaired assembly for the lack of some post-translational event or alteration of assembly factors [54]; indeed, the assembly of Complex I is very complex and not yet fully understood [55]. In addition, it has become clear that Complex I is unstable and becomes disassembled in absence of super-complex organization [56,57]. To this purpose, it is evident from 2D-electrophoresis (Fig. 6) that the low amount of Complex I present in transformed fibroblasts is mostly isolated and less assembled with Complex III and Complex IV in high molecular weight (MW) supercomplexes. In particular, the highest MW supercomplex (see Fig. 6, band d) detected in control cells is almost absent in ras-transformed fibroblasts. We have previously reported [58] that enhanced ROS generation induces dissociation of the I–III supercomplex with consequent lack of efficient electron channelling from Complex I to Complex III; moreover the concomitant disruption of Complex I assembly induced by supercomplex dissociation [56,57] might also account for the decrease of NAD-linked respiration and ATP synthesis. It is tempting to speculate that activation of ubiquitin-dependent and -independent degradation systems [59] would then be operative to eliminate the disassembled subunits. The OXPHOS dysfunction in K-ras transformed cells might then lead to compensatory enhancement of glycolysis to overcome the energetic deficiency.

In conclusion, the decrease of Complex I activity in ras-transformed fibroblasts appears to be sufficient to explain the impairment of mitochondrial function and the Warburg effect. Therefore, the observation here reported that Complex I activity is selectively reduced in K-ras cells as it is in other types of tumours [24], might indicate an alternative possible target in order to develop therapeutic approaches and/or cellular diagnosis for some type of cancers.

Acknowledgements

This work has been supported by grants from Alma Mater Studiorum, Università di Bologna, Progetti strategici di Ateneo E.F. 2005 to G.L., ITALBIONET to L.A., and FAR to F.C. The authors wish to thank Neil Campbell for language checking.

References

[1] R. Moreno-Sánchez, S. Rodríguez-Enríquez, A. Marín-Hernández, E. Saavedra, Energy metabolism in tumor cells, FEBS J. 274 (2007) 1393–1418.
[2] X.L. Zu, M. Guppy, Cancer metabolism: facts, fantasy, and fiction, Biochem. Biophys. Res. Commun. 313 (2004) 459–465.
[3] O. Warburg, On the origin of cancer cells, Science 123 (1956) 309–314.
[4] T. Pfeiffer, S. Schuster, S. Bonhoeffer, Cooperation and competition in the evolution of ATP-producing pathways, Science 292 (2001) 504–5077.
[5] R.J. Deberardinis, A. Mancuso, E. Daikhin, I. Nissim, M. Yudkoff, S. Wehrli, C.B. Thompson, Beyond aerobic glycolysis: transformed cells can engage in glutamine metabolism that exceeds the requirement for protein and nucleotide synthesis, Proc. Natl. Acad. Sci. USA 104 (2007) 19345–19350.
[6] N. Bellance, P. Lestienne, R. Rossignol, Mitochondria: from bioenergetics to the metabolic regulation of carcinogenesis, Front. Biosci. 14 (2009) 4015–4034.
[7] V. Gogvadze, S. Orrenius, B. Zhivotovsky, Mitochondria as targets for cancer chemotherapy, Semin. Cancer Biol. 19 (2009) 57–66.
[8] N.C. Denko, Hypoxia, HIF1 and glucose metabolism in the solid tumour, Nat. Rev. Cancer 8 (2008) 705–713.
[9] J.W. Kim, I. Tchernyshyov, G.L. Semenza, C.V. Dang, HIF 1-mediated expression of pyruvate dehydrogenase kinase: a metabolic switch required for cellular adaptation to hypoxia, Cell Metab. 3 (2006) 177–185.
[10] R. Fukuda, H. Zhang, J-W. Kim, L.A. Shimoda, C.V. Dang, G.L. Semenza, Regulation of COX subunit composition by HIF-1: a mechanism for optimizing the efficiency of respiration in hypoxic cells, Cell 129 (2007) 111–122.
[11] G.L. Semenza, Oxygen-dependent regulation of mitochondrial respiration by hypoxia-inducible factor 1, Biochem. J. 405 (2007) 1–9.
[12] D.C. Wallace, A mitochondrial paradigm of metabolic and degenerative diseases, aging, and cancer: a dawn for evolutionary medicine, Annu. Rev. Genet. 39 (2005) 359–407.
[13] F. Chiaradonna, E. Sacco, R. Manzoni, M. Giorgio, M. Vanoni, L. Alberghina, Ras-dependent carbon metabolism and transformation in mouse fibroblasts, Oncogene 25 (2006) 5391–5404.
[14] F. Chiaradonna, D. Gaglio, M. Vanoni, L. Alberghina, Expression of transforming K-Ras oncogene affects mitochondrial functions and morphology in mouse fibroblasts, Biochim. Biophys. Acta 1757 (2006) 1338–1356.
[15] S. Matoba, J.G. Kang, W.D. Patino, A. Wragg, M. Boehm, O. Gavrilova, P.J. Hurley, F. Bunz, P.M. Hwang, p53 regulates mitochondrial respiration, Science 312 (2006) 1650–1653.
[16] J.S. Modica-Napolitano, K.K. Singh, Mitochondrial dysfunction in cancer, Mitochondrion 4 (2004) 755–762.
[17] Y. Shidara, K. Yamagata, T. Kanamori, K. Nakano, J.Q. Kwong, G. Manfredi, H. Oda, S. Ohta, Positive contribution of pathogenic mutations in the mitochondrial genome to the promotion of cancer by prevention from apoptosis, Cancer Res. 65 (2005) 1655–1663.
[18] E. Hervouet, A. Cízková, J. Demont, A. Vojtísková, P. Pecina, N.L. Franssen-van Hal, J. Keijer, H. Simonnet, R. Ivánek, S. Kmoch, C. Godinot, J. Houstek, HIF and reactive

oxygen species regulate oxidative phosphorylation in cancer, Carcinogenesis 29 (2008) 1528–1537.
[19] M.L. Genova, A. Baracca, A. Biondi, G. Casalena, M. Faccioli, A.L. Falasca, G. Formiggini, G. Sgarbi, G. Solaini, G. Lenaz, Is supercomplex organization of the respiratory chain required for optimal electron transfer activity? Biochim. Biophys. Acta 1777 (2008) 740–746.
[20] J.S. Carew, P. Huang, Mitochondrial defects in cancer, Mol. Cancer 1 (2002) 9.
[21] C.V. Dang, G.L. Semenza, Oncogenic alterations of metabolism, Trends Biochem. Sci. 24 (1999) 68–72.
[22] S. Mazurek, E. Eigenbrodt, The tumor metabolome, Anticancer Res. 23 (2003) 1149–1154.
[23] R.A. Gatenby, R.J. Gillies, Why do cancers have high aerobic glycolysis? Nat. Rev. Cancer 4 (2004) 891–899.
[24] H. Simonnet, J. Demont, K. Pfeiffer, L. Guenaneche, R. Bouvier, U. Brandt, H. Schagger, C. Godinot, Mitochondrial complex I is deficient in renal oncocytomas, Carcinogenesis 24 (2003) 1461–1466.
[25] E. Bonora, A.M. Porcelli, G. Gasparre, A. Biondi, A. Ghelli, V. Carelli, A. Baracca, G. Tallini, A. Martinuzzi, G. Lenaz, G. Romeo, Defective oxidative phosphorylation in thyroid oncocytic carcinoma is associated with pathogenic mitochondrial DNA mutations affecting complexes I and III, Cancer Res. 66 (2006) 6087–6096.
[26] H. Simonnet, N. Alazard, K. Pfeiffer, C. Gallou, C. Beroud, J. Demont, R. Bouvier, H. Schagger, C. Godinot, Low mitochondrial respiratory chain content correlates with tumor aggressiveness in renal cell carcinoma, Carcinogenesis 23 (2002) 759–768.
[27] K. Buchet, C. Godinot, Functional F_1-ATPase essential in growth and membrane potential of human mitochondrial DNA-depleted ρ_0 cells, J. Biol. Chem. 273 (1998) 22985–22989.
[28] G.M. Cereghetti, L. Scorrano, The many shapes of mitochondrial death, Oncogene 25 (2006) 4717–4724.
[29] P. Huang, T. Yu, Y. Yoon, Mitochondrial clustering induced by overexpression of the mitochondrial fusion protein Mfn2 causes mitochondrial dysfunction and cell death, Eur. J. Cell Biol. 86 (2007) 289–302.
[30] L. Plecita-Hlavata, M. Lessard, J. Santorova, J. Bewersdorf, P. Jezek, Mitochondrial oxidative phosphorylation and energetic status are reflected by morphology of mitochondrial network in INS-1E and HEP-G2 cells viewed by 4Pi microscopy, Biochim. Biophys. Acta 1777 (2008) 834–846.
[31] P. Bossù, M. Vanoni, V. Wanke, M.P. Cesaroni, F. Tropea, G. Melillo, C. Asti, S. Porzio, P. Ruggiero, V. Di Cioccio, G. Maurizi, A. Ciabini, L. Alberghina, A dominant negative RAS-specific guanine nucleotide exchange factor reverses neoplastic phenotype in K-ras transformed mouse fibroblasts, Oncogene 19 (2000) 2147–2154.
[32] F. Yamamoto, M. Perucho, Activation of a human c-K-ras oncogene, Nucleic Acids Res. 12 (1984) 8873–8885.
[33] S. Kahn, F. Yamamoto, C. Almoguera, E. Winter, K. Forrester, J. Jordano, M. Perucho, The c-K-ras gene and human cancer (review), Anticancer Res. 7 (1987) 639–652.
[34] J.L. Bos, Ras oncogenes in human cancer: a review, Cancer Res. 49 (1989) 4682–4689.
[35] A.J. Dupuy, K. Morgan, F.C. Von Lintig, H. Shen, H. Acar, D.E. Hasz, N.A. Jenkins, N.G. Copeland, G.R. Boss, D.A. Largaespada, Activation of the Rap1 guanine nucleotide exchange gene, CalDAG-GEF I, in BXH-2 murine myeloid leukaemia, J. Biol. Chem. 276 (2001) 11804–11811.
[36] K.S. Vogel, K.S. Klesse, S. Velasco-Miguel, K. Meyers, E.J. Rushing, L.F. Parada, Mouse tumor model for neurofibromatosis type 1, Science 286 (1999) 2176–2179.
[37] J. Yun, C. Rago, I. Cheong, R. Pagliarini, P. Angenendt, H. Rajagopalan, K. Schmidt, J. K. Willson, S. Markowitz, S. Zhou, L.A. Diaz, V.E. Velculescu, C. Lengauer, K.W. Kinzler, B. Vogelstein, N. Papadopoulos, Glucose deprivation contributes to the development of KRAS pathway mutations in tumor cells, Science 325 (2009) 1555–1559.
[38] S. Pulciani, E. Santos, L.K. Long, V. Sorrentino, M. Barbacid, Ras gene amplification and malignant transformation, Mol. Cell Biol. 5 (1985) 2836–2841.
[39] G. Sgarbi, A. Baracca, G. Lenaz, L.M. Valentino, V. Carelli, G. Solaini, Inefficient coupling between proton transport and ATP synthesis may be the pathogenic mechanism for NARP and Leigh syndrome resulting from the T8993G mutation in mtDNA, Biochem. J. 395 (2006) 493–500.
[40] A. Baracca, G. Solaini, G. Sgarbi, G. Lenaz, A. Baruzzi, A.H. Schapira, A. Martinuzzi, V. Carelli, Severe impairment of complex I-driven adenosine triphosphate synthesis in leber hereditary optic neuropathy cybrids, Arch. Neurol. 62 (2005) 730–736.
[41] A. Baracca, G. Sgarbi, M. Mattiazzi, G. Casalena, E. Pagnotta, M.L. Valentino, M. Moggio, G. Lenaz, V. Carelli, G. Solaini, Biochemical phenotypes associated with the mitochondrial ATP6 gene mutations at nt8993, Biochim. Biophys. Acta-Bioenergetics 1767 (2007) 913–919.
[42] G. Solaini, G. Sgarbi, G. Lenaz, A. Baracca, Evaluating mitochondrial membrane potential in cells, Biosci Rep. 27 (2007) 11–21.
[43] A. Baracca, G. Sgarbi, G. Solaini, G. Lenaz, Rhodamine 123 as a probe of mitochondrial membrane potential: evaluation of proton flux through F(0) during ATP synthesis, Biochim. Biophys. Acta 1606 (2003) 137–146.
[44] A. Galmiche, J. Fueller, RAF kinases and mitochondria, Biochim. Biophys. Acta 1773 (2007) 1256–1262.
[45] S.J. Yeung, J. Pan, M.H. Lee, Roles of p53, Myc and HIF-1 in regulating glycolysis—the seventh hallmark of cancer, Cell Mol. Life Sci. 65 (2008) 3981–3999.
[46] A. Ramanathan, C. Wang, S.L. Schreiber, Perturbational profiling of a cell-line model of tumorigenesis by using metabolic measurements, Proc. Natl. Acad. Sci. USA 102 (2005) 5992–5997.
[47] Q. Tian, S.B. Stepaniants, M. Mao, L. Weng, M.C. Feetham, M.J. Doyle, E.C. Yi, H. Dai, V. Thorsson, J. Eng, D. Goodlett, J.P. Berger, B. Gunter, P.S. Linseley, R.B. Stoughton, R. Aebersold, S.J. Collins, W.A. Hanlon, L.E. Hood, Integrated genomic and proteomic analyses of gene expression in mammalian cells, Mol. Cell Proteomics 10 (2004) 960–969.
[48] A. Heddi, P. Lestienne, D.C. Wallace, G. Stepien, Coordinate induction of energy gene expression in tissues of mitochondrial disease patients, J. Biol. Chem. 274 (1999) 22968–22976.
[49] R.L. Terjung, The turnover of cytochrome *c* in different skeletal-muscle fibre types of the rat, Biochem. J. 178 (1979) 569–574.
[50] R.C. Hickson, M.A. Rosenkoetter, Separate turnover of cytochrome *c* and myoglobin in the red types of skeletal muscle, Am. J. Physiol. 241 (1981) C140–C144.
[51] A. Barrientos, C.T. Moraes, Titrating the effects of mitochondrial complex I impairment in the cell physiology, J. Biol. Chem. 274 (1999) 16188–16197.
[52] G. Lenaz, A. Baracca, R. Fato, M.L. Genova, G. Solaini, New insights into structure and function of mitochondria and their role in aging and disease, Antioxid. Redox Signal. 8 (2006) 417–437.
[53] A. Basoah, P.M. Matthews, K.J. Morten, Rapid rates of newly synthesized mitochondrial protein degradation are significantly affected by the generation of mitochondrial free radicals, FEBS Lett. 579 (2005) 6511–6517.
[54] D. De Rasmo, D. Panelli, A.M. Sardanelli, S. Papa, cAMP-dependent protein kinase regulates the mitochondrial import of the nuclear encoded NDUFS4 subunit of complex I, Cell Signal. 20 (2008) 989–997.
[55] R.O. Vogel, C.E. Dieteren, L.P. van den Heuvel, P.H. Willems, J.A. Smeitink, W.J. Koopman, L.G. Nijtmans, Identification of mitochondrial complex I assembly intermediates by tracing tagged NDUFS3 demonstrates the entry point of mitochondrial subunits, J. Biol. Chem. 282 (2007) 7582–7590.
[56] H. Schägger, R. De Coo, M.F. Bauer, S. Hofmann, C. Godinot, U. Brandt, Significance of respirasomes for the assembly/ stability of human respiratory chain complex I, J. Biol. Chem. 279 (2004) 36349–36353.
[57] M. D'Aurelio, C.D. Gajewski, G. Lenaz, G. Manfredi, Respiratory chain supercomplexes set the threshold for respiratory defects in human mtDNA mutant cybrids, Hum. Mol. Genet. 15 (2006) 2157–2169.
[58] G. Lenaz, M.L. Genova, Structural and functional organization of the mitochondrial respiratory chain: a dynamic super-assembly, Int. J. Biochem. Cell Biol. 41 (2009) 1750–1772.
[59] D. Germain, Ubiquitin-dependent and-independent mitochondrial protein quality controls: implications in ageing and neurodegenerative diseases, Mol. Microbiol. 70 (2008) 1334–1341.